18th Australasian Fluid Mechanics Conference
Launceston, Australia
3-7 December 2012

Reynolds-Averaged Navier-Stokes and Wall-Modelled Large-Eddy Simulations of Sonic Hydrogen Injection into Hypersonic Crossflow

R. M. Gehre, V. Wheatley, R. R. Boyce, D. M. Peterson and S. Brieschenk

Centre for Hypersonics
University of Queensland, QLD 4072, Australia

Abstract

The combustion efficiency in supersonic combustion ramjets (scramjets) is strongly dependent on the fuel injection process. This paper investigates the transverse injection of hydrogen into a hypersonic air crossflow at Mach 6 . The flow physics are investigated using both Reynolds-averaged Navier-Stokes (RANS) simulations and wall-modelled large-eddy simulations (WMLES). We focus on the comparison of the results of these two methods and their agreement with experimental temperature measurements. Assessing the performance of RANS and its shortcomings in this context is of particular interest due to its significantly reduced computational costs and its widespread use in the hypersonics community compared to WMLES.

Introduction

The need to increase the efficiency of propulsion systems at high Mach numbers has lead to the development of supersonic combustion ramjets (scramjets). One of the major challenges in supersonic combustion is achieving a high combustion efficiency, which is often limited by the mixing efficiency. A stoichiometric fuel-air mixture is desirable for combustion [7], and achieving a high mixing efficiency is important. The mixing process and thus the mixing efficiency are strongly dependent on the fuel injection method. Commonly, porthole injection is used to supply the scramjet with fuel [14, 9, 6, 2, 17]; however, a large variety of other injection methods, such as slot injection, injection behind a backward facing step and injection through a hypermixer have been investigated as well [7, 12]. This paper focuses on porthole injection, in particular on the numerical simulation of the fuel-air mixing process employing two different numerical simulation techniques, Reynold-averaged Navier-Stokes (RANS) simulations and wall-modeled large-eddy simulations (WMLES). RANS simulations are widespread in the hypersonic community due to their low computational resource requirements. Viti et al. [19] used RANS to investigate the main flow physics that are governing the porthole injection process and has shown that quasi-steady flow phenomena, such as shock structures and mean vortical structures, can be resolved well with RANS. Several studies that investigate porthole injection experimentally [1, 18] or with high fidelity numerical methods, such as large-eddy simulation (LES) [8, 13], show that inherently unsteady flow processes, such as vortex shedding, are occurring during the injection process. These unsteady flow features cannot be captured with RANS and must be modeled. Hence, analyzing injection flow fields solely with RANS can lead to a distorted perception of the true flow physics and, depending on modeling accuracy, can result in discrepancies between numerical and experimental results.

To address this issue, sonic hydrogen injection into Mach 6 crossflow has been analyzed employing two numerical methods, RANS and WMLES. The resulting averaged temperature distributions at the jet symmetry plane are compared with experimental data. In particular, the distribution of hydrogen is of importance, since it has a major influence on the temperature distribution and further downstream on the combustion process. We focus on features of the hydrogen distribution that RANS modeling fails to predict accurately.

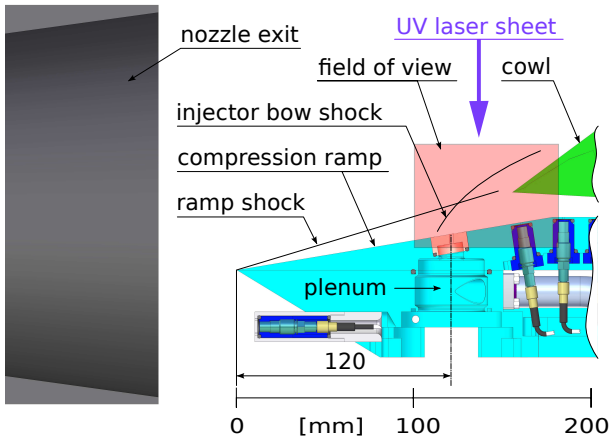

Figure 1: Experimental arrangement to scale [3].

Experimental setup

Figure 1 shows the sonic hydrogen injection experiment, which is part of a scramjet experiment. For clarity, only a brief description of the experimental details relevant to the injection experiment is given. The experimental campaign was conducted in the T-ADFA free piston shock-tunnel at the University of New South Wales, Australian Defence Force Academy. The shock-tunnel provides high enthalpy flow, which is accelerated though a conical nozzle, displayed in Figure 1, to hypersonic speeds. At the nozzle exit the freestream reaches a temperature T_∞ of 140 K, a pressure p_∞ of 675 Pa, a velocity u_∞ of 2063 m/s and a Mach number M_∞ of ~ 9. The hypersonic freestream impinges on the 9° compression ramp of the scramjet generating an oblique shock wave as depicted in Figure 1. The flow conditions behind the shock wave are the following: $T = 275$ K, $p = 3850$ Pa, $u = 1995$ m/s and $M \sim 6$. A 1.6 mm diameter porthole, which is located 120 mm downstream of the scramjet leading edge, angled at 81° to the flow along the compression ramp is used to inject sonic hydrogen with a plenum pressure of $p_{pl} = 2075$ Pa into supersonic crossflow. The planar laser-induced fluorescence (PLIF) technique is used measure temperatures at the jet symmetry plane by using the NO-molecules present in the freestream (NO-PLIF). This measurement technique is non-intrusive and thus well suited for this particular application. Figure 2 displays the ensemble averaged temperature measurements. For more information, the reader is referred to Brieschenk et al.[3].

Numerical method

The injector experiment is simulated using US3D, a research code developed at the University of Minnesota [11]. Both RANS and WMLES method are incorporated into the code. The improved delayed detached-eddy-simulation (IDDES) method,

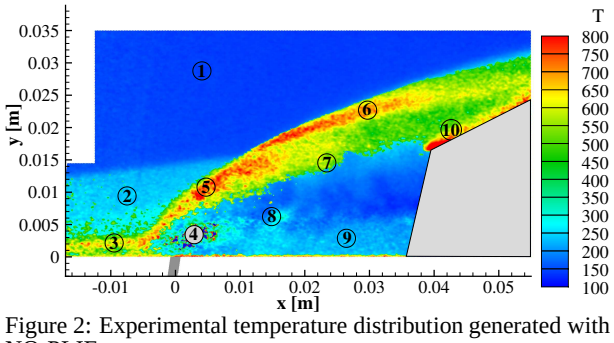

Figure 2: Experimental temperature distribution generated with NO-PLIF.

which is described in detail by Peterson et al. [13], is used for WMLES. The Spalart-Allmaras turbulence model [15] is used to close the RANS equations and as the background RANS model for IDDES [16]. To account for chemical non-equilibrium effects, the 12-species Evans-Schexnayder finite-rate chemistry model [5] is incorporated into US3D.

To achieve the best agreement with the experimental data the nozzle flow has been simulated to generate accurate inflow conditions for the scramjet model. Also, the entire scramjet inlet has been modeled. A preliminary investigation has shown that the corner vortices, which develop at the intersection between the inlet compression ramp and the sidewalls, do not influence the jet interaction flow field at the centerline. Therefore, only the region near the centerline, where the jet plume is present, is well resolved. With increasing distance from the centerline the spanwise resolution decreases to reduce the computational costs. The mesh has a total of 29,061,028 cells. At the injector orifice the cell sizes (edge length) are smaller than 0.04 mm. With increasing distance from the injector the cell sizes increase to $0.15mm$. The chosen grid spacing ensures that more than 80% of the turbulence kinetic energy is resolved, which indicates sufficient spacial resolution [10]. The mesh is clustered towards the walls to achieve $y^+ < 1$, resolving the developing boundary layer. The time step used for WMLES is set to $5 \times 10^{-9} s$ to time accurately resolve the shear-layer development region. The time-average of the WMLES is calculated over 50,000 iteration, thus over $250\mu s$.

Results

This section analyses the temperature distribution generated by the jet interaction. Furthermore, a comparison between the numerical and experimental data is conducted.

Figure 2 shows the experimentally determined ensemble-average temperature distribution at the jet symmetry plane. To aid discussion, Fig. 2 is annotated with numbers from 1 to 10, each representing a specific zone in the temperature map. The relative position of the temperature map in reference to the overall experiment can be seen in Fig. 1. The flow enters the domain on the left hand side. Zone 1 and 2 are positioned in the freestream and in the post-leading-edge-shock region, respectively. The hydrogen injection creates a blockage in the flow field, causing a bow-shock, a barrel shock (4) and an upstream separation zone (3). The volume enclosed by the barrel shock (4) contains pure hydrogen, which means that no meaningful temperatures can be measured in the region using NO-PLIF. A Similar problem occurs for region 8, which represents the hydrogen plume region. Hence, large errors in the temperatures are induced due to the marginal amounts of NO present. The large temperature gradient observable in zone 7 is caused by the cooling effect of the hydrogen plume. The measurement sensitivity for this transition region is, however, very low [3], which is inherent to the way the experimental measurements are obtained. Further measurements would be necessary to increase the sensitivity in this region. Hence, the temperatures in zone 7 are unreliable and thus not usable for comparison, which is unfortunate since the effect of vortex shedding on the temperature distribution can not be analyzed. Region 10 shows the influence of the scramjet cowl, present in the experiment, which has not been incorporated into the numerical simulation. Therefore, the temperature measurements in this region should be disregarded. Furthermore, the area underneath the cowl is not penetrated by the laser sheet resulting in no temperature information.

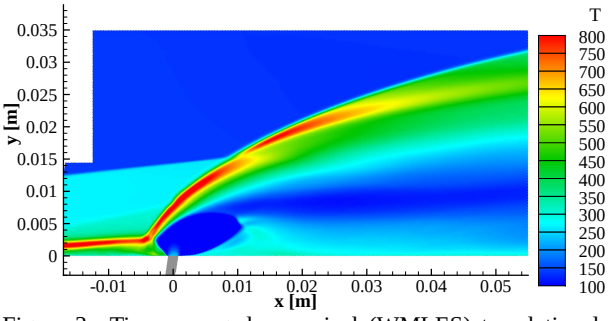

Figure 3: Time-averaged numerical (WMLES) translational-rotational temperature distributions in the jet symmetry plane.

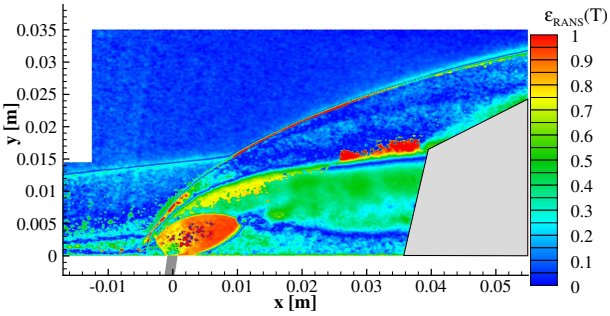

Figure 4: Relative error between the experimental and numerical (RANS) translational-rotational temperature distributions in the jet symmetry plane.

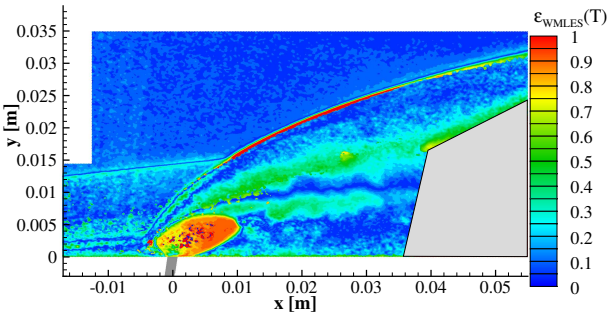

Figure 5: Relative error between the experimental and numerical (WMLES) translational-rotational temperature distributions in the jet symmetry plane.

Figure 3 shows the numerically generated temperature distribution, using WMLES, in the jet symmetry plane, which agrees well with the experimental data. For better comparison, Fig. 4 and 5 display the relative error between the numerical and experimental temperature distribution for RANS and WMLES, respectively. The qualitative agreement between the numerical and experimental results is excellent. The shock shapes, shock positions and size of the separation zone are captured well by both RANS and WMLES. The quantitative temperature comparison, however, shows discrepancies. Taking the limitations of the experimental setup into consideration, leaves zones 1, 2, 3, 5, 6 and 9 for comparison. The quantitative agreement of the numerical data with the experimental data is excellent for zone 1, 2 and 6, considering the experimental uncertainties [3]. The relative error in the remaining zones is increased; however, the

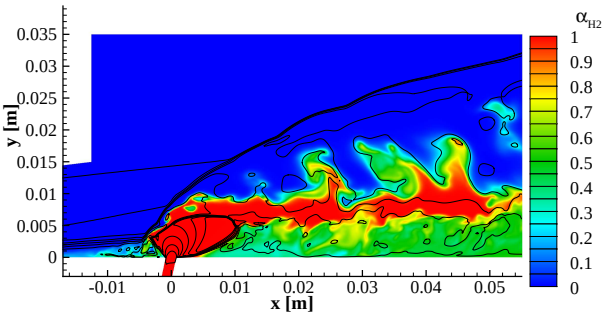

Figure 6: Instantaneous hydrogen distribution on the jet symmetry plane superimposed with Mach number contour lines from 1 to 7 generated with WMLES.

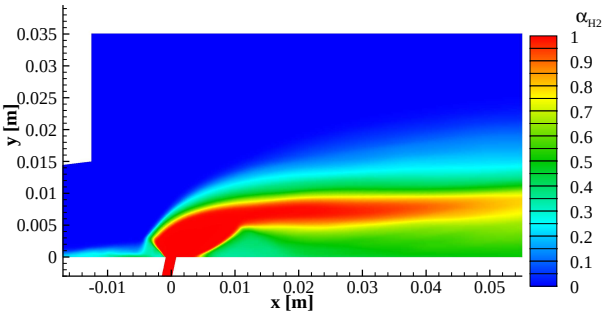

Figure 7: Time-averaged hydrogen distribution on the jet symmetry plane generated with WMLES.

measurement uncertainties [3], not shown here, in this region are large as well. Nevertheless, the WMLES results show better quantitative agreement than the RANS results. We believe this is due to the unsteady effects that cannot be captured with RANS and will be discussed further in the following section.

Analysis and discussion

This section analyses the discrepancies between the numerical temperature maps in conjunction with the hydrogen distribution. Significant differences between the RANS and WMLES methods and their impact on the flow physics will be discussed. Also, the mixing efficiency downstream of the injection is analyzed.

Separation zone

Figure 6 shows an instantaneous hydrogen distribution on the jet symmetry plane from the WMLES. The focus should be placed on the separated region (3) upstream of the barrel shock. This region contains two vortices; one small counter-clockwise rotating vortex adjacent to the jet, which entrains cold hydrogen from the jet into the clockwise rotating vortex generated by the boundary-layer separation. It can be seen that a significant amount of hydrogen is present in the the separation zone. This process decreases the temperature within the separation zone leaving only a thin high temperature region on top of the separation zone. This detail can also be seen in the experimental temperature measurements shown in Fig. 2. The hydrogen entrainment into the recirculation region is governed by an unsteady shedding motion. Therefore, it is not resolvable by RANS. Figures 8 and 7 display the time-average hydrogen distribution on the jet symmetry plane generated with RANS and WMLES, respectively.

From Fig. 7, it is apparent that a significant amount of hydrogen is entrained into the separation zone in the WMLES, whereas Fig. 8 shows only small amounts of hydrogen. Hence, RANS under-predicts the amount of hydrogen within the separation, which results in higher temperatures due to the decreased cooling effect. This leads to the WMLES temperature distribution

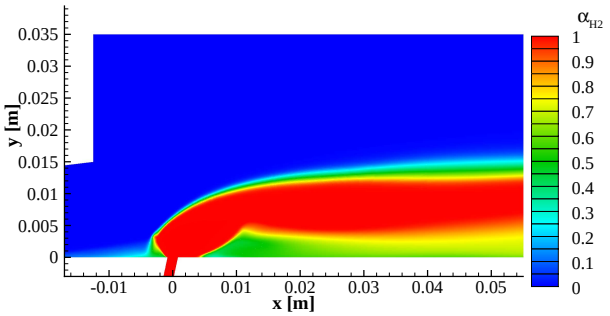

Figure 8: Hydrogen distribution on the jet symmetry plane generated with RANS.

agreeing better with the experimental results in the upstream separation.

Shock unsteadiness

The aforementioned unsteadiness of the jet, which causes the hydrogen shedding, also effects the bow shock. Near the barrel shock, where the influence of the unsteadiness is largest, significant movement of the shock structure is observable as can be seen in Fig. 6. The perturbations in the Mach number contour lines representing the bow shock dampen out with increasing wall normal distance. At the steepest part of the bow shock, where the unsteady effects are strongest, high temperatures of up to $1500K$ are present in the flow field (5). These high temperature spots change position over time due to the unsteadiness of the bow shock, which results in a lower average temperature of roughly $900K$. Again, WMLES agrees much better with the experimental data than RANS, which predicts temperatures that are similar to the instantaneous temperatures.

Mixing region

A shear layer forms between the hydrogen jet and the cross-flow, causing strong vortex shedding events to occur. Figure. 6 demonstrates how the instantaneous hydrogen distribution deviates significantly from the average one. Similar to the separation zone, shear layer vortices transport cool hydrogen into regions above the mean jet plume causing the temperature to decrease. As mentioned before, this flow region can unfortunately not be analyzed due to experimental constrains. The mixing induced by the lower hydrogen shear-layer (9) can be investigated, however. The hydrogen shedding events are not as dominant as for the top shear-layer, but significant mixing still occurs. Hence, cold hydrogen mixes with the air creating a well mixed, but cold, fuel-air mixture. WMLES resolves the unsteady mixing process well and shows great quantitative agreement for this region. RANS, however, over-predicts the temperatures due to an under-prediction of the mixing process.

Mixing efficiency

To finalize the analysis, the hydrogen distributions for the cross-flow plane 25 jet-diameters (40 mm) downstream of the injector, shown in Fig. 9, are compared with each other. Fig. 9 clearly shows the major differences between the RANS and WMLES. Again, a highly unsteady, asymmetric and distorted hydrogen distribution is present in the instantaneous WMLES flow field. The modeling of these physical processes has a major influence on the mixing performance. This fact becomes readily apparent when comparing the time-averaged WMLES and RANS hydrogen distributions. The overall shape is similar, but RANS predicts a very compact hydrogen distribution, which can be considered largely unmixed, whereas WMLES shows a clearly diffused distribution, due to time-averaging hydrogen shedding events, indicating better mixing. It should be noted that the time-averaged WMLES hydrogen distribution is a misleading

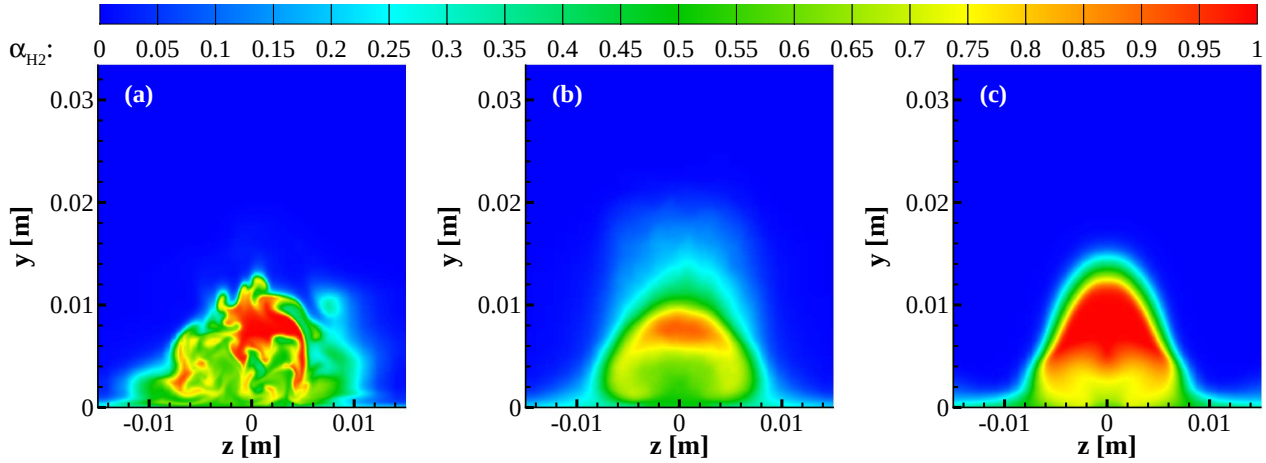

Figure 9: An a) instantaneous (WMLES) b) averaged WMLES and c) RANS hydrogen distribution at a cross-flow plane 25 jet-diameters downstream of injector.

representation of the mixing process [18], but yet helpful to identify mixing regions. The mixing efficiency [4] at the aforementioned crossflow plane is 14.9% and 9.1% using WMLES and RANS, respectively. Thus RANS under-predicts the mixing efficiency, compared to WMLES, by more than 60%, which is an unphysical representation of the mixing process. The RANS results can be improved by adjusting the turbulent Schmidt-number to increase the turbulent transport and thus increase the mixing rate. This measure would, however, be dependent on the specific test case and cause rather unphysical diffusive mixing, since the turbulent mass transport is modeled through a turbulent mass diffusion model.

Conclusions

The results presented clearly show the advantage of WMLES over RANS for the simulation of a jet in supersonic crossflow. The overall qualitative distributions are very similar, but quantitatively large discrepancies arise where unsteady effects dominate the flow physics. RANS is not capable of capturing vortex shedding, which affects the temperature distribution in the separation zone and the mixing region. Furthermore, the mixing process is largely under-predicted resulting in low mixing efficiencies, at least for the computational modeling used in this study. These results indicate that WMLES is necessary to correctly predict the mixing processes in scramjets.

Acknowledgements

The authors would like to thank Professor Graham Candler's research group for providing the CFD research code. The research is funded by the Australian Space Research Program. This work was supported by an award under the Merit Allocation Scheme on the NCI National Facility at the ANU.

References

[1] Ben-Yakar, A. and Hanson, R. K., Ultra-fast-framing schlieren system for studies of the time evolution of jets in supersonic crossflows, *Experiments in Fluids*, **32**, 2002, 652–666.

[2] Boyce, R. R., Schloegel, F., McIntyre, T. J. and Tirtey, S. C., Pressure-scaling of inlet-injection radical-farming scramjets, in *20th International Symposium on Airbreathing Engines*, 2011.

[3] Brieschenk, S., Gehre, R. M., Wheatley, V., Boyce, R. R., Kleine, H. and OByrne, S., Jet interaction in a hypersonic flow: A comparison between plif thermometry and computational simulation, ICAS, 2012, 28^{th} International Congress of the Aeronautical Sciences.

[4] Doster, J. C., King, P. I., Gruber, M. R., Carter, C. D., Ryan, M. and K.Hsu, In-stream hypermixer fueling pylons in supersonic flow, *Journal of Propulsion and Power*, **25**, 2009, 885–901.

[5] Evans, J. S. and Schexnayder, Jr., C. J., Influence of Chemical Kinetics and Unmixedness on Burning in Supersonic Hydrogen Flames, *AIAA Journal*, **18**, 1980, 188–193.

[6] Gardner, A., Paull, A. and McIntyre, T., Upstream porthole injection in a 2-d scramjet model, *Shock Waves*, **11**, 2002, 369375.

[7] Heiser, W. H. and Pratt, D. T., *Hypersonic Airbreathing Propulsion*, AIAA Education Series, 1994.

[8] Kawai, S. and Lele, S. K., Large-eddy simulation of jet mixing in supersonic crossflows, *AIAA Journal*.

[9] McGuire, J. R., Boyce, R. R. and Mudford, N. R., Radical farm ignition processes in two-dimensional supersonic combustion, *Journal of Propulsion and Power*, **24**, 2008, 1248–1257.

[10] Naudin, A., Vervisch, L. and Domingo, P., A turbulent-energy based mesh refinement procedure for large eddy simulation, in *Advances in Turbulence XI*, editors J. Palma and A. S. Lopes, Springer Berlin Heidelberg, 2007, volume 117 of *Springer Proceedings in Physics*, 413–415, 10.1007/978-3-540-72604-3_130.

[11] Nompelis, I., Drayna, T. W. and Candler, G. V., Development of a hybrid unstructured implicit solver for the simulation of reacting flows over complex geometries, in 34^{th} *AIAA Fluid Dynamics Conference*, Portland, 2004.

[12] Pandey, K. and Sivasakthivel, T., Recent advances in scramjet fuel injection - a review, *International Journal of Chemical Engineering and Applications*, **1**, 2010, 294–301.

[13] Peterson, D. M. and Candler, G. V., Hybrid reynolds-averaged and large-eddy simulation of normal injection into a supersonic crossflow, *Journal of Propulsion and Power*, **26**, 2010, 533–544.

[14] Smart, M. K. and Hass, N. E., Flight data analysis of the hyshot 2 scramjet flight experiment, *AIAA Journal*, **44**, 2006, 2366–2375.

[15] Spalart, P. R. and Allmaras, S. R., One-equation turbulence model for aerodynamic flows, *Rech Aerosp*, 5–21.

[16] Subbareddy, P. K. V., *Stable Low-Dissipation Schemes for Turbulent Compressible Flows*, Ph.D. thesis, University of Minnesota, 2007.

[17] Turner, J. C. T., *An Experimental Investigation of Inlet Fuel Injection in a Three-Dimensional Scramjet Engine*, Ph.D. thesis, University of Queensland, Brisbane, Australia, 2010.

[18] VanLerberghe, W. M., Santiago, J. G., Dutton, J. C. and Lucht, R. P., Mixing of a sonic transverse jet injected into a supersonic flow, *AIAA Journal*, **38**, 2000, 470–479.

[19] Viti, V., Neel, R. and Schetz, J. A., Detailed flow physics of the supersonic jet interaction flow field, *Physics of Fluids*, **21**, 2009, 046101.